Clean Technol., Vol. 30, No. 3, September 2024, pp. 258-266

청정에너지기술 보 문

Utilizing SnO_2 Encapsulated within a Freestanding Structure of N-Doped Carbon Nanofibers as the Anode for High-Performance Lithium-Ion Batteries

Ying Liu[1,2†], Jungwon Heo[1†], Dong-Ho Baek[1], Mingxu Li[3], Ayeong Bak[1], Prasanth Raghavan[4], Jae-Kwang Kim[2*], and Jou-Hyeon Ahn[1,3*]

[1]Department of Chemical Engineering, Gyeongsang National University
Jinju 52828, Republic of Korea
[2]Department of Energy Convergence Engineering, Cheongju University
285 Daseong-ro, Cheongju 28503, Republic of Korea
[3]Department of Materials Engineering and Convergence Technology, Gyeongsang National University
Jinju 52828, Republic of Korea
[4]Department of Polymer Science and Rubber Technology, Cochin University of Science and Technology
Kochi, 682022, India

(Received for review May 21, 2024; Revision received July 1, 2024; Accepted July 2, 2024)

Abstract

Rechargeable Li-SnO_2 batteries suffer from issues such as poor electronic/ionic conductivity and huge volume changes. In order to overcome these inherent limitations, this study designed a cell with a unique hierarchical structure, denoted as SnO_2@PCNF. The SnO_2@PCNF cell design incorporates *in-situ* generated SnO_2 nanoparticles strategically positioned within N-doped porous carbon nanofibers (PCNF). The *in-situ* generated SnO_2 nanoparticles can alleviate strains during cycling and shorten the pathway for the ions and electrons, improving the utilization of active materials. Moreover, the N-doped PCNF establishes a continuously conductive network to further increase the electrical conductivity and also buffers the significant volume changes that occur during charging and discharging. The resulting SnO_2@PCNF cell exhibits outstanding electrochemical performance and stable cycling characteristics. Notably, a reversible capacity of 520 mAh g^{-1} was achieved after 100 cycles at 70 mA g^{-1}. Even under a higher current density of 1 A g^{-1}, the cell maintained a capacity retention of 393 mAh g^{-1} after 1,000 cycles. These results highlight the SnO_2@PCNF cell's exceptional cycling stability and superior rate capability.

Keywords : SnO_2, Nitrogen doping, Porous carbon nanofiber, Rechargeable Li-SnO_2 batteries

1. Introduction

Lithium-ion batteries (LIBs) have captured significant research interest as promising devices for energy storage applications, owing to their high energy density, low self-discharge, long cycle life, and absence of memory effects[1-3]. However, traditional LIBs utilizing graphite as the anode material face challenges in meeting the escalating demands for higher energy density, given the low theoretical capacity of graphite[4-6]. Therefore, the development of advanced anode materials with higher theoretical capacities is crucial to overcoming the current limitations of LIBs. Silicon, tin, titanium oxide, cobalt oxide, and tin oxide are among the candidates being explored. Among these, tin-based materials have garnered significant attention due to their high theoretical capacities, cost-effectiveness, and abundant availability. Metallic tin (Sn) boasts an impressive specific theoretical capacity of 994 mAh g^{-1}. Additionally, tin oxides (SnO_x), particularly SnO_2 and SnO, are considered potential next-generation anode materials, attributed to their superior theoretical capacities of 1,494 mAh g^{-1} and 1,273 mAh g^{-1}, respectively[7,8]. However, practical applications of Sn-based anode materials in LIBs encounter obstacles, including poor electronic/ionic conductivity and significant volume changes (>300%) during the alloying/de-alloying processes[9,10]. These challenges can lead to the pulverization and, consequently, severe capacity fading.

To address these challenges, researchers have developed a range

†These two authors contributed equally to this work.
*To whom correspondence should be addressed.
E-mail: jaekwang@cju.ac.kr, Tel: +82-43-883-4788
E-mail: jhahn@gnu.ac.kr, Tel: +82-55-772-1784, Fax: +82-55-772-1789
https://doi.org/10.7464/ksct.2024.30.3.258 pISSN 1598-9712 eISSN 2288-0690

of techniques, including manipulating the morphology of SnO_2 and integrating carbon matrices with SnO_2. The former involves preparing SnO_2 with diverse morphologies, such as nanobelts[11], nanoparticles[12], and hollow spheres[13], to enhance reversible capacities. However, the cycle performance of these SnO_2 structures has been hindered by inferior results, primarily due to the huge volume expansion during cycling processes, which can lead to the structural pulverization and collapse. Consequently, the latter method has gained widespread attention in recent years. The integration of carbon serves as a buffering mechanism, allowing for the accommodation of huge volume changes while simultaneously enhancing electrical conductivity. For example, Spada et al. reported a self-supported fibrous Sn/SnO_2@C composite using the electrospinning method, exhibiting improved reaction kinetics and cycling stability. This composite demonstrated a remarkable capacity retention of 300 mAh g^{-1} over 500 cycles at 0.5 A g^{-1}[14]. In another study, Saddique et al. synthesized a Sn/SnO_2/C nanocomposite via a low-cost hydrothermal method, showing a high initial reversible discharge capacity (2,248 mAh g^{-1}) at 100 mA g^{-1}. Furthermore, it displayed excellent capacity retention of 474.6 mAh g^{-1} at a high current density of 500 mA g^{-1} after 100 cycles[15]. Evidently, the adoption of a well-thought-out structural design proves to be a highly effective approach for enhancing the electrochemical performance of Li-SnO_2 batteries.

Relative to pristine carbon, the introduction of heteroatoms (S, N, and P) into carbon can significantly enhance its electrical conductivity, facilitating the efficient transfer of Li ions within the cell[16,17]. Furthermore, carbon nanofibers, as a subclass of one-dimensional (1D) carbonaceous materials boasting excellent electronic conductivity, serve as an exceptional carbon matrix. Accordingly, we elaborately engineered a hierarchical structure (SnO_2@PCNF) wherein SnO_2 nanoparticles were encapsulated within N-doped porous carbon nanofibers (PCNF). This synthesis involved a facile incipient wetness technique and an *in-situ* oxidation process, effectively addressing all pertinent challenges associated with rechargeable Li-SnO_2 batteries. The N-doped PCNF, characterized by high electronic conductivity, a large surface area, and robust structural stability, plays a pivotal role in enhancing conductivity, expediting electron transfer, and mitigating volume expansion. Simultaneously, the *in-situ* formed SnO_2 nanoparticles exhibit improved properties, such as alleviating strains during lithiation and delithiation processes and shortening the pathway for ions and electrons. Additionally, the 1D carbon fiber matrices establish a continuous 3D conductive network, further improving electrical conductivity. Consequently, the unique hierarchical structure of the SnO_2@PCNF anode material exhibits exceptional cycling performance and rate capability. It achieves an outstanding lithiation capacity retention of 520 mAh g^{-1} at 70 mA g^{-1} after 100 cycles and maintains a superior capacity of 393 mAh g^{-1} at a high current density of 1 A g^{-1} even after 1,000 cycles. The freestanding hierarchical SnO_2@PCNF composite exhibits remarkable electrochemical performance and cycling stability, positioning it as a promising anode material for advanced LIBs.

2. Materials and methods

2.1 Materials

Polyacrylonitrile (PAN, average MW 150,000, Sigma-Aldrich), Polystyrene (PS, Yakuri Pure Chemicals Co., Ltd.), N, N-dimethylformamide (DMF, 99.0%; Samchun Pure Chemical Co., Ltd.), tin (II) chloride dihydrate ($SnCl_2{\cdot}2H_2O$, 98.0%, Sigma-Aldrich), Poly(ethylene glycol)-b-poly(propylene glycol)-b-poly(ethylene glycol) (P123, Mn 5800, Sigma-Aldrich), hydrochloric acid (HCl, 35.0 ~ 37.0%, Samchun Pure Chemical Co., Ltd.), hydrofluoric acid (HF, 48.0 ~ 51.0%, AvantorTM Performance Materials), tetraethyl orthosilicate (TEOS, 99.0%, Sigma-Aldrich), and N-methylpyrrolidone (NMP, 99.5%, Samchun Pure Chemical Co., Ltd.) were used as received.

2.2 Preparation of SnO_2@PCNF and pSnO_2 composites

The synthesis of freestanding SnO_2@PCNF involved several steps, beginning with the preparation of an N-doped porous carbon nanofiber (PCNF) through modifications to a previous study[18]. Initially, PS was dissolved in DMF at 60 °C with continuous stirring until complete dissolution. Subsequently, a specific amount of polyacrylonitrile (PAN) was added to the PS solution with stirring. The resulting PS/PAN solution was then loaded into a syringe equipped with a 21-gauge metallic needle. Applying a high voltage of 17 kV and a flow rate of 5 mL h^{-1}, electrospinning was performed with the collector fixed at a distance of 20 cm from the metallic needle. The obtained PAN/PS fiber was subjected to stabilization at 300 °C for 3 h in an air atmosphere, followed by carbonization at 800 °C for 5 h under an argon atmosphere, utilizing a heating rate of 3 °C min^{-1}. In the PAN/PS solution, PS forms a microemulsion that stretches into nanoscale wires within the PAN fibers during electrospinning. Upon carbonization at 800 °C in an argon atmosphere, the PS decomposes, creating parallel channels within the carbonized PAN shells[18,19]. This process results in the formation of N-doped porous carbon nanofibers (PCNF). Subsequently, $SnCl_2{\cdot}2H_2O$ was dissolved in an ethanol/distilled water mixture (v/v = 8/2). After complete dissolution of $SnCl_2{\cdot}2H_2O$, a white milky solution was obtained. A predetermined quantity of PCNF was introduced into the solution, and the mixture

was agitated in a shaking water bath at 50 °C for 12 h. Following washing, the $SnCl_2·2H_2O$@PCNF composite was subjected to calcinate at 300 °C for 4 h in an air atmosphere. This final step led to the formation of the freestanding SnO_2@PCNF composite.

In order to enable a comprehensive comparison of electrochemical performance, porous SnO_2 nanorods ($pSnO_2$) were synthesized in accordance with a previously reported procedure[20]. A pre-prepared solution of $SnCl_2·2H_2O$ was carefully dropped onto SBA-15 template. The resulting mixture of $SnCl_2·2H_2O$ and SBA-15 powder was subjected to heating at 90 °C for 12 h to ensure complete impregnation. The composite was then calcined at 500 °C for 4 h in an air atmosphere. Subsequently, the mixture underwent treatment in a 5% HF solution for 30 min to eliminate the SBA-15. The resulting material was washed with distilled water several times to remove residual impurities. Ultimately, the $pSnO_2$ were successfully obtained.

2.3 Characterization of materials

The morphologies and internal structures of the prepared samples were characterized through field-emission scanning electron microscopy (FE-SEM, TESCAN, MIRA3 LM) and transmission electron microscopy (TEM, FEI, TF30ST). The specific surface area and pore volume were quantified using Brunauer-Emmet-Teller analysis (BET, Micromeritics, ASAP 2010). The crystal structures of the synthesized samples were studied employing X-ray diffraction (XRD, Bruker, D2 Phaser). To determine the SnO_2 mass ratio within the SnO_2@PCNF composite, thermogravimetric analysis (TGA, TA Instruments, Q50) was conducted over a temperature range from room temperature to 600 °C, employing a heating rate of 10 °C min^{-1} under an O_2 atmosphere.

2.4 Electrochemical characterization

The freestanding SnO_2@PCNF fiber mat was cut into circular discs with a diameter of 10 mm and a SnO_2 loading of approximately 1.3 mg cm^{-2}, facilitating direct utilization as an electrode. For comparison, a slurry comprising 80 wt% $pSnO_2$, 10 wt% polyvinylidene fluoride (PVdF), and 10 wt% Super P in NMP was coated onto copper foil and subsequently dried at 80 °C for 12 h under vacuum. The coated material was then punched into 10 mm diameter circles with a similar SnO_2 loading mass as the SnO_2@PCNF, for use as electrodes. The electrolyte employed in the experiments consisted of 1 M lithium hexafluorophosphate ($LiPF_6$) dissolved in a mixture of ethylene carbonate (EC) and diethylene carbonate (DEC) in a volume ratio of 1:1. Stainless steel (SS) Swagelok® cells were assembled within an argon-filled glove box, utilizing lithium metal foil as the counter electrode, Celgard® 2400 as the separator, and the prepared SnO_2@PCNF or $pSnO_2$ electrode as the anode. Galvanostatic charge/discharge tests and cyclic voltammetry (CV) measurements were conducted using a WBCS3000 battery cycler (WonA Tech. Co., Ltd., South Korea) within a voltage range of 0.01 ~ 3.0 V (vs. Li/Li^+). Electrochemical impedance spectroscopy (EIS) was performed employing an impedance analyzer (ZIVE SP2, WonA Tech. Co., Ltd.) across a frequency range of 0.1 Hz to 100 Hz.

3. Results and discussion

A straightforward and scalable approach was employed to synthesize the freestanding porous SnO_2@PCNF anode material, as illustrated in Figure 1. The PCNF reveals a smooth surface and fibrous morphology, characterized by a uniform diameter of approximately ~1 μm, as depicted in Figure 2(a, b). The magnified cross-section image of PCNF in Figure 2c shows numerous parallel channels, providing ample storage space. The highly parallel channels in PCNF are clearly observed in Figure 2d, consistent with the cross-sectional view in Figure 2c. Following the encapsulation of SnO_2, the SEM and TEM images in Figure 2(e, f) highlight the parallel channel structure of SnO_2@PCNF. The presence of internal void spaces not only serves to buffer the volume changes of SnO_2 during lithiation and delithiation processes but also effectively enhances electrolyte accessibility, providing easily traversable diffusion pathways for ion transport. Energy dispersive X-ray spectroscopy (EDS) mapping of SnO_2@PCNF (Figure 2g) reveals the homogeneous distribution of SnO_2 within the PCNF carbon matrix. In contrast, the $pSnO_2$ composite (Figure 2(h, i)) exhibits a short rod shape with a diameter of approximately

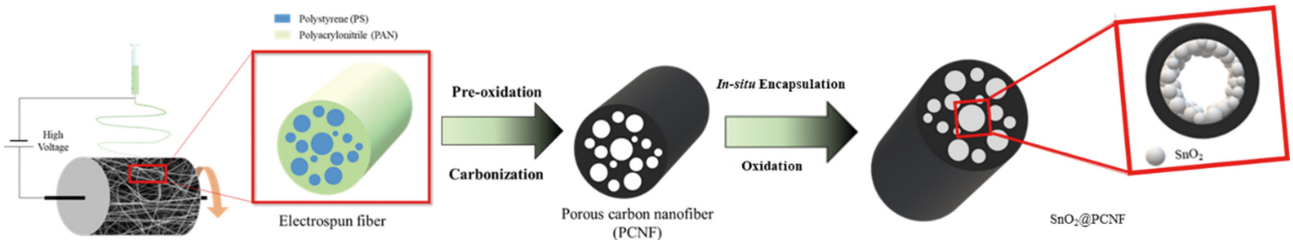

Figure 1. Illustration of the sequential fabrication steps for SnO_2@PCNF composite.

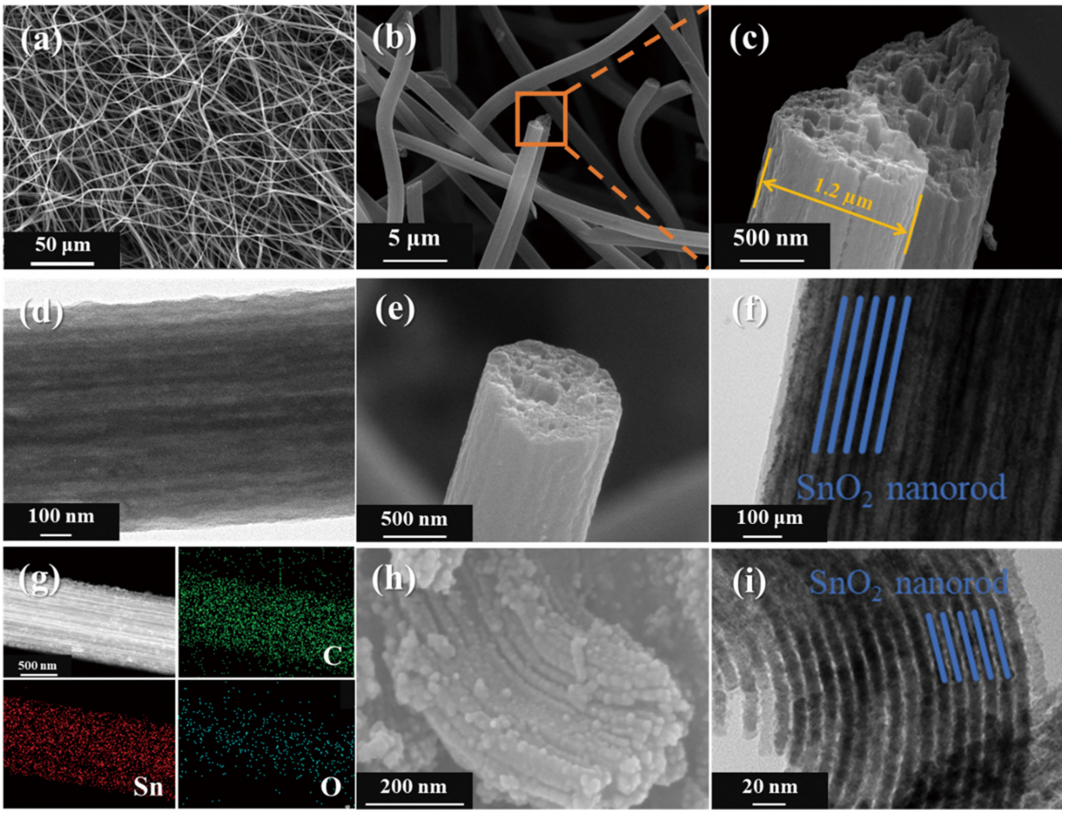

Figure 2. (a-c) FE-SEM images of PCNF, (d) TEM image of PCNF, (e-f) SnO_2@PCNF, (g) EDS mapping of SnO_2@PCNF, (h) FE-SEM image of $pSnO_2$, and (i) TEM image of $pSnO_2$.

~300 nm and highly ordered parallel mesoporous channels in the one-dimensional space.

The N_2 adsorption/desorption isotherms for PCNF, SnO_2@PCNF, and $pSnO_2$ composites are illustrated in Figure 3a. PCNF exhibited a typical type II and type IV isotherm with an H3 type hysteresis loop, indicating the presence of a large number of tube-shaped pores. In comparison to the as-synthesized PCNF, the specific surface area of SnO_2@PCNF significantly decreased from 461 m^2g^{-1} to 278 m^2g^{-1}, suggesting the successful incorporation of SnO_2 into the channels of PCNF. Nevertheless, the *in-situ* generated SnO_2 did not entirely occupy the channels of PCNF based on the BET result of SnO_2@PCNF, indicating a feature that may assist in alleviating the volume changes undergone by SnO_2 during both charge and discharge processes, which was aligned with the observations in Figure 2(e, f). Additionally, $pSnO_2$ exhibited the lowest specific surface area, measuring at 82 m^2g^{-1}. The XRD analysis in Figure 3b facilitated the identification of phases in PCNF, SnO_2@PCNF, and $pSnO_2$ composites. The XRD patterns of $pSnO_2$ exhibited a high match with the standard diffraction peaks of tetragonal SnO_2 (JCPDS 41-1445). In the case of PCNF, a broad peak at 25.8°, corresponding to the (002) plane of amorphous carbon, was observed. The main diffraction peaks at 26.6, 33.8, 37.9 and 51.8° of SnO_2@PCNF aligned well with the (110), (101), (200) and (211) crystal planes of SnO_2, devoid of any noticeable impurities, signifying complete conversion of the precursor to SnO_2. Using the Scherrer equation, the crystallite size of SnO_2 in SnO_2@PCNF is 4.1 nm. To obtain the accurate content of SnO_2 in the SnO_2@PCNF composite, TGA was performed in an O_2 atmosphere from room temperature to 600 °C (Figure 3c). The significant mass loss was observed from 350 to 550 °C, attributed to the oxidation of carbon within the SnO_2@PCNF composite[21]. Finally, the estimated SnO_2 content in the SnO_2@PCNF composite was approximately 47 wt%.

The electrochemical behavior of SnO_2@PCNF and $pSnO_2$ electrodes is elucidated through the CV curves presented in Figure 4(a, b). In the initial cathodic scan for both samples, the voltage hysteresis (Peak I) is attributed to the formation of a solid electrolyte interface (SEI) film on the active material surfaces and irreversible electrolyte decomposition[22,23]. It is noteworthy that the current value of $pSnO_2$ (peak I) significantly surpasses that of SnO_2@PCNF, signifying a greater magnitude of irreversible reactions in $pSnO_2$. This implies that the well-designed structure of SnO_2@PCNF effectively mitigates the occurrence of irreversible reactions in the first lithiation process, thereby enhancing the initial Coulombic efficiency and active material utilization[24]. In the subsequent cycles, the lithiation voltage undergoes a shift to a higher value (Peak II), corresponding to the reduction process

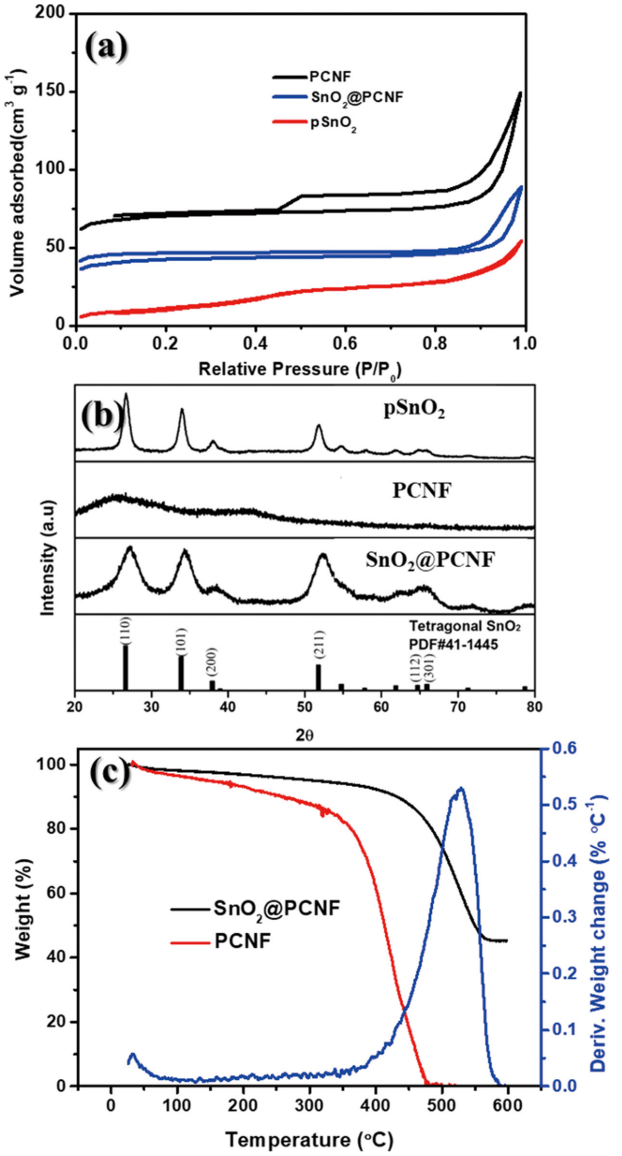

Figure 3. (a) Nitrogen adsorption-desorption isotherms, (b) XRD patterns of PCNF, SnO_2@PCNF, $pSnO_2$, and (c) TGA plot of PCNF, SnO_2@PCNF composites.

from SnO_2 to Sn (Equation (1)). Another lithiation voltage (Peak III) is associated with the alloying reaction from Sn to Li-Sn alloy (Equation (2)). The anodic peaks (Peak IV and Peak V) are indicative of the oxidation reaction from Li-Sn to Sn, and further to SnO_2[25,26]. The current value of SnO_2@PCNF (Peak III) exceeds that of $pSnO_2$, suggesting a more complete occurrence of the alloying reaction. Additionally, it is observed that Peaks II and III of SnO_2@PCNF exhibit consistent repeatability in the CV curves, indicating a stable reaction environment. This stability further emphasizes the advantageous features of the SnO_2@PCNF structure in promoting reliable and repeatable electrochemical processes.

$$SnO_2 + 4Li^+ + 4e^- \leftrightarrow Sn + 2Li_2O \quad (1)$$

$$Sn + xLi^+ + xe^- \leftrightarrow Li_xSn (0 \le x \le 4.4) \quad (2)$$

The $pSnO_2$ cell initially demonstrated a high lithiation capacity of 1,861 mAh g^{-1} at 70 mA g^{-1}. Moreover, a notable irreversible capacity observed after the first cycle, attributed to the irreversible reactions. In the subsequent cycles (Figure 4c), capacity degradation occurred due to the pulverization of $pSnO_2$ nanoparticles during the lithiation-delithiation processes. On the other hand, the SnO_2@PCNF cell exhibited a significant initial lithiation capacity of 1,364 mAh g^{-1} at 70 mA g^{-1} (Figure 4d), and from the 2nd cycle, the SnO_2@PCNF cell maintained a capacity retention of approximately 800 mAh g^{-1}, indicating that SnO_2@PCNF cell possesses excellent repeatability and cyclability. The extended cycling performance of $pSnO_2$ and SnO_2@PCNF cells is illustrated in Figure 4e. After 100 cycles at 70 mA g^{-1}, the SnO_2@PCNF cell demonstrated a remarkable capacity retention of around 520 mAh g^{-1} and a Coulombic efficiency of approximately 100%. In contrast, the $pSnO_2$ cell exhibited a significantly lower retained capacity of only 91 mAh g^{-1} after the same number of cycles, highlighting that SnO_2@PCNF effectively enhances the reversibility of the conversion reaction. A rate capability test for SnO_2@PCNF was conducted, as depicted in Figure 4f. The SnO_2@PCNF cell started at a current density of 0.1 A g^{-1} for 5 cycles, progressively increased to 1 A g^{-1}, and then decreased back to 0.1 A g^{-1}. Initial lithiation capacities of 628, 485, 384, 356, and 441 mAh g^{-1} were achieved at current densities of 0.1, 0.2, 0.5, 1, and 0.1 A g^{-1}, respectively. The superior rate capability of the SnO_2@PCNF composite can be attributed to its unique structure. The porous architecture not only serves to buffer volume changes but also enhances electrolyte accessibility, facilitating ion transfer within the cell and promoting a stable reversible reaction process[27]. Furthermore, the long cycling performance of the SnO_2@PCNF cell was evaluated at a high current density of 1 A g^{-1} (Figure 4g). Impressively, a lithiation capacity retention of 393 mAh g^{-1} was maintained even after 1000 cycles, accompanied by a Coulombic efficiency of approximately 100%. The electrochemical performance of SnO_2@PCNF surpasses that of previously reported SnO_2/carbon composites, as demonstrated in Table 1[28-32]. These findings emphasize the effectiveness of the unique hierarchical structure in the SnO_2@PCNF composite, which can address challenges inherent in rechargeable Li-SnO_2 batteries, exhibiting exceptional rate capability, prolonged lifetime, and superior cycling performance.

After cycling, the magnified morphology of the $pSnO_2$ electrode distinctly reveals the collapse and subsequent agglomeration of the porous structure compared to the fresh electrode (Figure 5(a, b)). This phenomenon is attributed to the sever volume changes

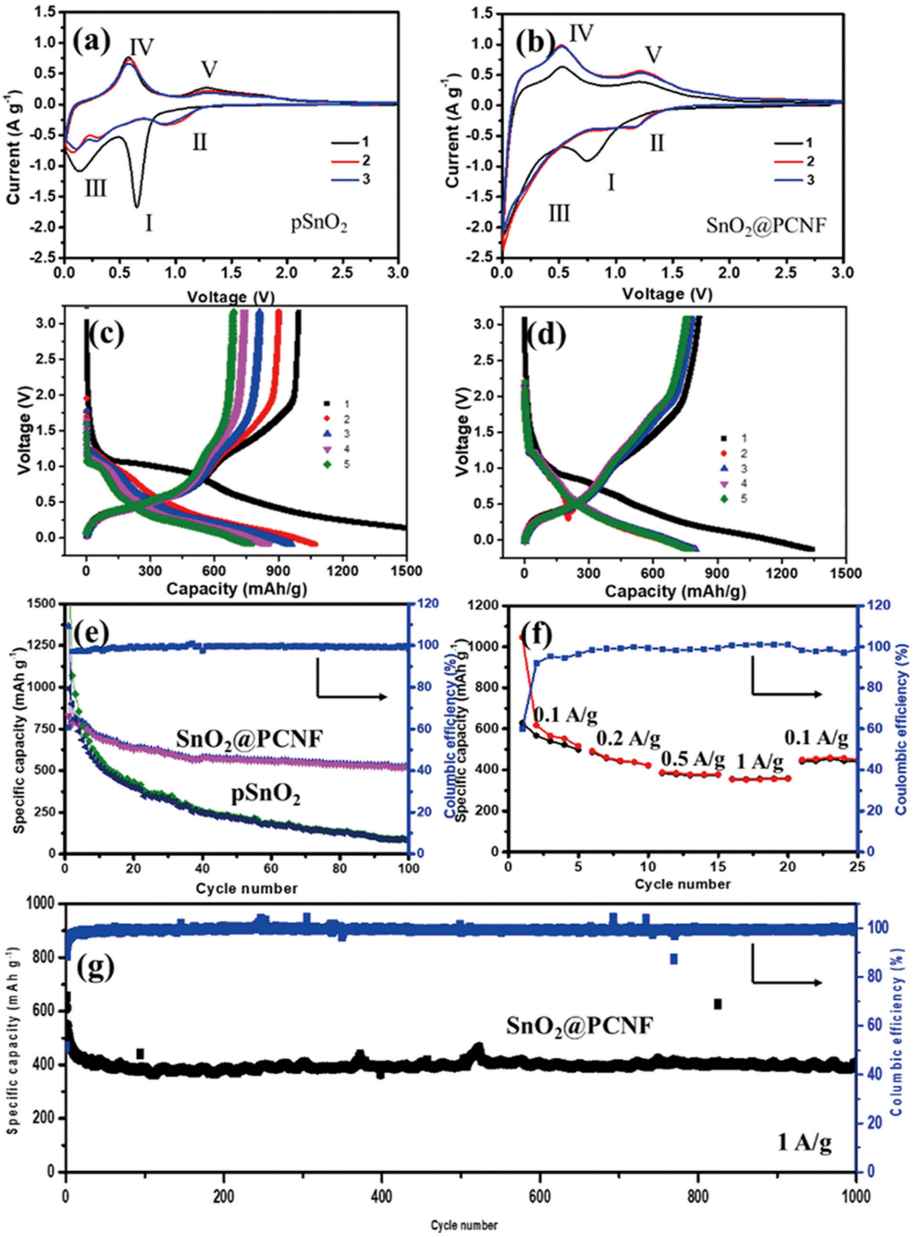

Figure 4. CV curves of (a) $pSnO_2$, (b) SnO_2@PCNF (scan rate: 0.1 mV s^{-1}; 0.01 ~ 3.0 V), charge-discharge profiles of (c) $pSnO_2$, (d) SnO_2@PCNF, (e) cycling performances and Coulombic efficiency of $pSnO_2$ and SnO_2@PCNF cells at 70 mA g^{-1}, (f) rate performances of SnO_2@PCNF, (g) long cycling performances and Coulombic efficiency of SnO_2@PCNF cell at 1 A g^{-1}.

Table 1. Summary of previous studies on SnO_2/carbon composite-based anode for LIBs

Anode material employed	Current density (mA g^{-1})	Initial lithiation capacity (mAh g^{-1})	Retained lithiation capacity (mAh g^{-1})	Cycles	Refs
Flexible SnO_2/G-CNT paper	100	990	387	50	28
SnO_2/G-CNT	100	1,050	502	50	29
SnO_2/G-CNT	200	1,806	842	40	30
SnO_2-G	50	2,140	649	30	31
SnO_2/gC	50	1,675	592	100	32
SnO_2/MWNT	50	907	231	50	
SnO_2@PCNF	70	1,364	520	100	This work
	1,000	653	393	1,000	

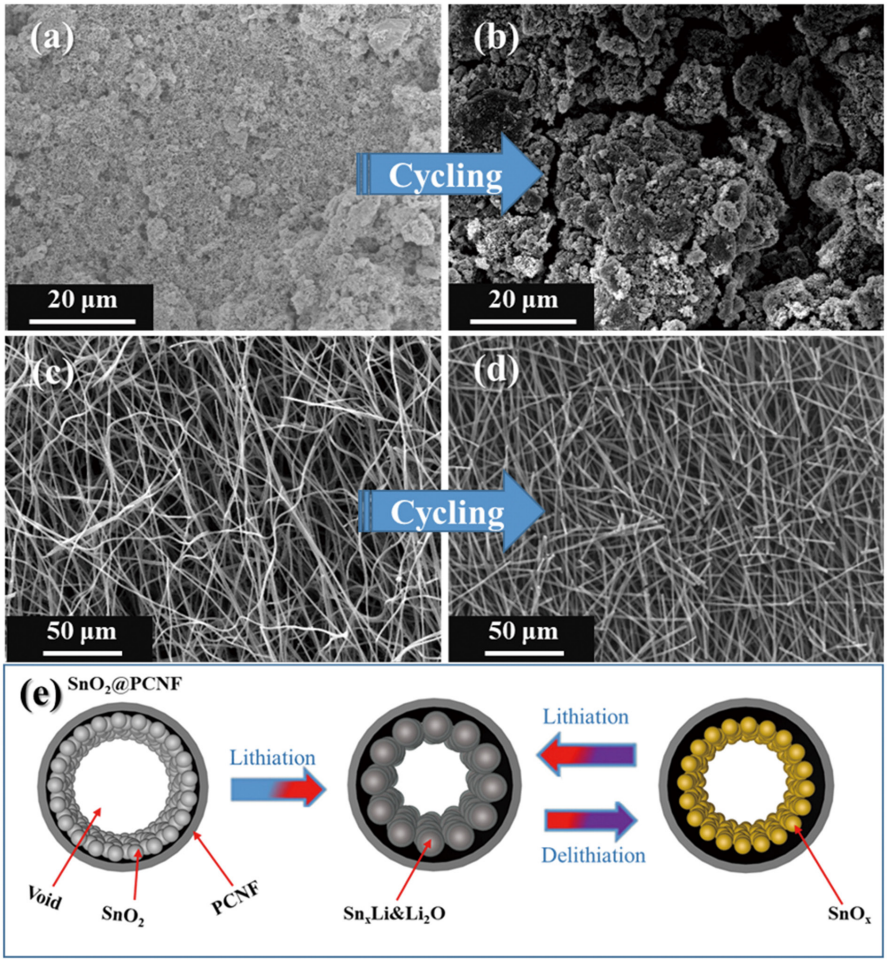

Figure 5. FE-SEM morphologies of (a) fresh $pSnO_2$ electrode, (b) $pSnO_2$ electrode after 50 cycles, (c) fresh SnO_2@PCNF electrode, (d) SnO_2@PCNF electrode after 50 cycles, and (e) schematic illustration showing the reaction processes of SnO_2@PCNF electrode.

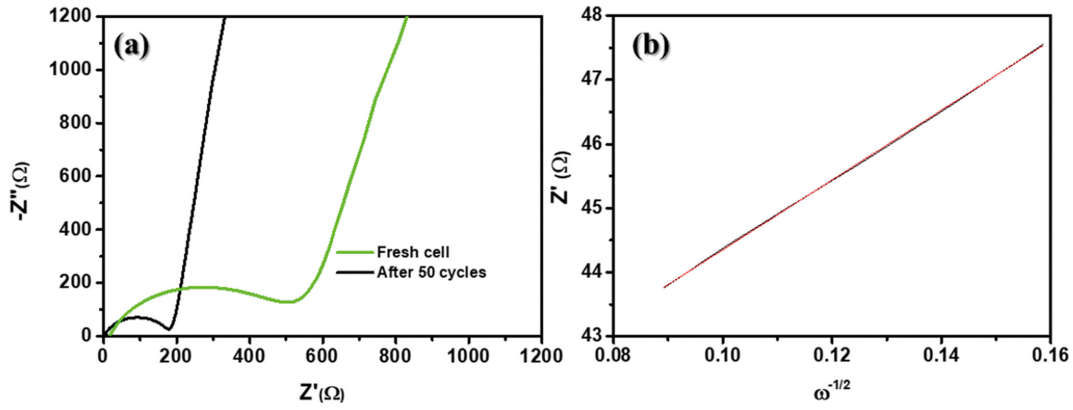

Figure 6. (a) EIS spectra of the SnO_2@PCNF cell, (b) relationship between the real part resistance and the inverse square root of the angular speed in the low-frequency range for the cycled SnO_2@PCNF cell.

experienced during cycles, potentially leading to rapid capacity fading. In contrast, the magnified morphology of the SnO_2@PCNF electrode in both the fresh and cycled states (Figure 5(c, d)) exhibits no significant differences, suggesting the maintenance of good structural integrity. As illustrated in Figure 5e, the *in-situ* generated SnO_2 can be can be securely embedded within the PCNF, providing additional voids to accommodate the volume changes of SnO_2 during (de)lithiation processes. Moreover, the PCNF, characterized by its 1D fibrous structure, serves to enhance electrical conductivity and optimize reaction kinetics.

The EIS spectra of the SnO_2@PCNF cell were obtained in the fully delithiated state both before and after cycling (Figure 6).

The Nyquist plots of the SnO_2@PCNF cell exhibit a depressed semicircle in the high-middle frequency region, indicative of the charge transfer process (R_{ct}), and a slope line in the low frequency range, where the Warburg impedance (R_w) signifies the diffusion process of Li^+ ions[33]. The R_{ct} of the cycled SnO_2@PCNF cell is significantly lower (215 Ω) compared to that of the fresh cell (708 Ω), demonstrating a notable decrease in resistance during the charge transfer processes. This suggests enhanced rapid reaction kinetics due to better electrolyte accessibility. Figure 6b shows a plot of the real part resistance versus the inverse square root of the angular speed in the low-frequency range for the cycled SnO_2@PCNF cell. The Warburg factor (σ) is obtained from the slope and substituted into Equation (3),

$$D = \frac{R^2T^2}{2A^2n^2F^4C^2\sigma^2} \quad (3)$$

where R is the gas constant, T is the absolute temperature, A is the electrode surface area, F is the Faraday constant, and C is the molar concentration of Li ions in the active material. Consequently, the lithium diffusion coefficient (D) of the cycled SnO_2@PCNF cell is calculated to be 3.12×10^{-11} cm^2 s^{-1}, confirming the rapid reaction kinetics in the SnO_2@PCNF cell.

4. Conclusions

A well-designed hierarchical structured SnO_2@PCNF composite was synthesized through a facile incipient wetness technique and an *in-situ* oxidation process. The excellent cycling performance and superior rate capability obtained, were attributed to (1) the 1D carbon fiber establishes a 3D continuous conductive network, reinforcing electrical conductivity and improving reaction kinetics, and (2) the porous structure of the SnO_2@PCNF composite buffers volume changes during lithiation and delithiation processes, enhances electrolyte accessibility, and facilitates ion transfer, and (3) the *in-situ* generated SnO_2 alleviates (de)lithiation strains, accelerating ion/electron transfer. Consequently, even at high current densities, the designed SnO_2@PCNF composite exhibits high reversible capacity, long cycle life, superior rate capability, and excellent cycling stability. This study provides inspiration for the rational design of anode materials for Li-ion batteries, contributing to the further development of high-performance energy-storage systems.

Acknowledgements

This research was supported by 'regional innovation mega project' program through the Korea Innovation Foundation funded by Ministry of Science and ICT (Project Number: 2023-DD-UP-0026) and the National Research Foundation of Korea (NRF) grant funded by the Korea government (MSIT) (No. RS-2023-00217581).

References

1. Bernard, P., Alper, J. P., Haon, C., Herlin-Boime, N., and Chandesris, M., "Electrochemical Analysis of Silicon Nanoparticle Lithiation-effect of Crystallinity and Carbon Coating Quantity," *J. Power Sources*, **435**, 226769 (2019).
2. Autthawong, T., Yodbunork, C., Ratsameetammajak, N., Namsar, O., Chimupala, Y., and Sarakonsri, T., "Enhanced Electrochemical Performance of Sn(SnO_2)/TiO_2(B) Nanocomposite Anode Materials with Ultrafast Charging and Stable Cycling for High-Performance Lithium-ion Batteries," *ACS Appl. Energy Mater*., **5**, 13829-13842 (2022).
3. Sun, C. R. and Kim, J. H., "Development of Bismuth Alloy-based Anode Material for Lithium-ion Battery," *Clean Technol.*, **30**, 23-27 (2024).
4. Zhu, Y., Huang, Y., and Wang, M., "Three-dimensional Hierarchical Porous $MnCo_2O_4$@MnO_2 Network Towards Highly Reversible Lithium Storage by Unique Structure," *Chem. Eng. J.*, **378**, 122207 (2019).
5. Zhang, W., Wang, B., Luo, H., Jin, F., Ruan, T., and Wang, D., "MoO_2 Nanobelts Modified with an MOF-derived Carbon Layer for High Performance Lithium-ion Battery Anodes," *J. Alloys Compd*., **803**, 664-670 (2019).
6. Kim, Y. B. and Park, G. D., "Synthesis of Porous-structured (Ni, Co)Se_2-CNT Microsphere and Its Electrochemical Properties as Anode for Sodium-ion Batteries," *Clean Technol.*, **29**, 178-184 (2023).
7. Dai, L., Zhong, X., Zou, J., Fu, B., Su, Y., Ren, C., Wang, J., and Zhong, G., "Highly Ordered SnO_2 Nanopillar Array as Binder-free Anodes for Long-life and High-rate Li-ion Batteries," *Nanomaterials*, **11**, 1307 (2021).
8. Zhou, S., Zhou, H., Zhang, Y., Zhu, K., Zhai, Y., Wei, D., and Zeng, S., "SnO_2 Anchored in S and N co-doped Carbon as the Anode for Long-life Lithium-ion Batteries," *Nanomaterials*, **12**, 700 (2022).
9. Zoller, F., BÖhm, D., Bein, T., and Fattakhova-Rohlfing, D., "Tin Oxide Based Nanomaterials and Their Application as Anodes in Lithium-ion Batteries and Beyond," *ChemSusChem*, **12**, 4140-4159 (2019).
10. Cheng, Y., Wang, S., Zhou, L., Chang, L., Liu, W., Yin, D., Yi, Z., and Wang, L., "SnO_2 Quantum Dots: Rational Design to Achieve Highly Reversible Conversion Reaction and Stable Capacities for Lithium and Sodium Storage," *Small*, **16**, 2000681 (2020).
11. Comini, E., Faglia, G., Sberveglieri, G., Pan, Z., and Wang,

Z. L., "Stable and Highly Sensitive Gas Sensors Based on Semiconducting Oxide Nanobelts," *Appl. Phys. Lett*., **81**, 1869-1871 (2002).

12. Gu, F., Wang, S. F., Lü, M. K., Zhou, G. J., Xu, D., and Yuan, D. R., "Photoluminescence Properties of SnO_2 Nanoparticles Synthesized by Sol-gel Method," *J. Phys. Chem. B*, **108**, 8119-8123 (2004).
13. Wu, P., Du, N., Zhang, H., Zhai, C., and Yang, D., "Self-templating Synthesis of SnO_2-Carbon Hybrid Hollow Spheres for Superior Reversible Lithium Ion Storage," *ACS Appl. Mater. Interfaces*, **3**, 1946-1952 (2011).
14. Spada, D., Bruni, P., Ferrari, S., Albini, B., Galinetto, P., Berbenni, V., Girella, A., Milanese, C., and Bini, M., "Self-supported Fibrous Sn/SnO_2@C Nanocomposite as Superior Anode Material for Lithium-ion Batteries," *Materials*, **15**, 919 (2022).
15. Saddique, J., Shen, H., Ge, J., Huo, X., Rahman, N., Mushtaq, M., Althubeiti, K., and Al-Shehri, H., "Synthesis and Characterization of Sn/SnO_2/C Nano-composite Structure: High-performance Negative Electrode for Lithium-ion Batteries," *Materials*, **15**, 2475 (2022).
16. Liu, Y., Zhao, X., Chauhan, G. S., and Ahn, J. H., "Nanostructured Nitrogen-doped Mesoporous Carbon Derived from Polyacrylonitrile for Advanced Lithium Sulfur Batteries," *Appl. Surf. Sci*., **380**, 151-158 (2016).
17. Yuan, Y., Chen, Z., Yu, H., Zhang, X., Liu, T., Xia, M., Zheng, R., Shui, M., and Shu, J., "Heteroatom-doped Carbon-based Materials for Lithium and Sodium Ion Batteries," *Energy Storage Mater*., **32**, 65-90 (2020).
18. Li, Z., Zhang, J. T., Chen, Y. M., Li, J., and Lou, X. W. D., "Pie-like Electrode Design for High-energy Density Lithium-sulfur Batteries," *Nat. Commun*., **6**, 8850 (2015).
19. Ishita, I. and Singhal, R., "Porous Multi-channel Carbon Nanofiber Electrodes Using Discarded Polystyrene Foam as Sacrificial Material for High-performance Supercapacities," *J. Appl. Electrochem.*, **50**, 809-820 (2020).
20. Heo, J., Liu, Y., Haridas, A. K., Jeon, J., Zhao, X., Cho, K. K., Ahn, H. J., Lee, Y., and Ahn, J. H., "Carbon-Coated Ordered Mesoporous SnO_2 Composite Based Anode Material for High Performance Lithium-Ion Batteries," *J. Nanosci. Nanotechnol*., **18**, 6415-6421 (2018).
21. Ambalkar, A. A., Panmand, R. P., Kawade, U. V., Sethi, Y. A., Naik, S. D., Kulkarni, M. V., Adhyapak, P. V., and Kale, B. B., "Facile Synthesis of SnO_2@carbon Nanocomposites for Lithium-ion Batteries," *New J. Chem*., **44**, 3366-3374 (2020).
22. Wang, Z., Chen, L., Feng, J., Liu, S., Wang, Y., Fan, Q., and Zhao, Y., "In-situ Grown SnO_2 Nanospheres on Reduced GO Nanosheets as Advanced Anodes for Lithium-ion Batteries," *ChemistryOpen*, **8**, 712-718 (2019).
23. Chen, J. S., Cheah, Y. L., Chen, Y. T., Jayaprakash, N., Madhavi, S., Yang, Y. H., and Lou, X. W., "SnO_2 Nanoparticles with Controlled Carbon Nanocoating as High-Capacity Anode Materials for Lithium-ion Batteries," *J. Phys. Chem. C*, **113**, 20504-20508 (2009).
24. Tian, Z., Zhao, J., Li, B., Feng, Y., Song, J., Niu, C., Shao, L., and Zhang, W., "Controllable Synthesis of 3D Porous SnO_2/Carbon Towards Enhanced Lithium-ion Batteries," *Ionics*, **26**, 2773-2779 (2020).
25. Liang, J., Yu, X. Y., Zhou, H., Wu, H. B., Ding, S., and Lou, X. W., "Bowl-like SnO_2@carbon Hollow Particles as an Advanced Anode Material for Lithium-ion Batteries," *Angew. Chem. Int. Ed*., **53**, 12803-12807 (2014).
26. Liu, M., Zhang, S., Dong, H., Chen, X., Gao, S., Sun, Y., Li, W., Xu, J., Chen, L., Yuan, A., and Lu, W., "Nano-SnO_2/Carbon Nanotube Hairball Composite as a High-Capacity Anode Material for Lithium Ion Batteries," *ACS Sustainable Chem. Eng*., **7**, 4195-4203 (2019).
27. Narsimulu, D., Nagaraju, G., Sekhar, S. C., Ramulu, B., and Yu, J. S., "Three-Dimensional Porous SnO_2/carbon Cloth Electrodes for High-performance Lithium- and Sodium-ion Batteries," *Appl. Surf. Sci*., **538**, 148033 (2021).
28. Zhang, B., Zheng, Q. B., Huang, Z. D., Oh, S. W., and Kim, J. K., "SnO_2-graphene-carbon Nanotube Mixture for Anode Material with Improved Rate Capacities," *Carbon*, **49**, 4524-4534 (2011).
29. Chen, T., Pan, L., Liu, X., Yu, K., and Sun, Z., "One-step Synthesis of SnO_2-reduced Graphene Oxide-carbon Nanotube Composites via Microwave Assistance for Lithium Ion Batteries," *RSC Adv.*, **2**, 11719-11724 (2012).
30. Zhang, Z., Wang, L., Xiao, J., Xiao, F., and Wang, S., "One-pot Synthesis of Three-Dimensional Graphene/carbon Nanotube/SnO_2 Hybrid Architectures with Enhanced Lithium Storage Properties," *ACS Appl. Mater. Interfaces*, **7**, 17963-17968 (2015).
31. Zhu, X., Zhu, Y., Murali, S., Stoller, M. D., and Ruoff, R. S., "Reduced Graphene Oxide/tin Oxide Composite as an Enhanced Anode Material for Lithium Ion Batteries Prepared by Homogenous Coprecipitation," *J. Power Sources*, **196**, 6473-6477 (2011).
32. Sahoo, M. and Ramaprabhu, S., "Solar Synthesized Tin Oxide Nanoparticles Dispersed on Graphene Wrapped Carbon Nanotubes as a Li Ion Battery Anode Material with Improved Stability," *RSC Adv.*, **7**, 13789-13797 (2017).
33. Liu, Y., Ju, H. C., Cho, K. K., Ahn, H. J., and Ahn, J. H., "Grape-cluster-like Hierarchical Structure of FeS_2 Encapsulated in Graphitic Carbon as Cathode Material for High-rate Lithium Batteries," *Appl. Surf. Sci*., **630**, 157458 (2023).